Solar Energy Materials & Solar Cells 117 (2013) 285–292

Contents lists available at SciVerse ScienceDirect

Solar Energy Materials & Solar Cells

journal homepage: www.elsevier.com/locate/solmat

Self-organization polymer consisting of quinacridone and quaterthiophene units: Coplanar structure between benzene and thiophene linkage

Ho Jun Song [a], Doo Hun Kim [a], Min Hee Choi [a], Soo Won Heo [a], Joo Young Lee [a], Jang Yong Lee [b], Doo Kyung Moon [a,*]

[a] Department of Materials Chemistry and Engineering, Konkuk University, 1 Hwayang-dong, Gwangjin-gu, Seoul 143-701, Republic of Korea
[b] Energy Materials Research Center, Korea Research Institute of Chemical Technology, P.O. Box 107, Yuseong, Daejeon 305-600, Republic of Korea

ARTICLE INFO

Article history:
Received 16 January 2013
Received in revised form
20 May 2013
Accepted 27 May 2013
Available online 11 July 2013

Keywords:
Quinacridone
Self-organization
OPVs
Conjugated polymer

ABSTRACT

Poly[quinacridone-co-quaterthiophene] (PQCQT) was synthesized through a Suzuki coupling reaction by introducing the characterization and self-assembly of quinacridone and quaterthiophene derivatives. The PQCQT was dissolved in a common organic solvent with an M_n value of 52.9 kg/mol. The optical band gap energy of the PQCQT was similar to the P3HT at 2.12 eV. The energy of the HOMO of the PQCQT was −5.10 eV, and the energy of the LUMO was −2.98 eV. The results of the X-ray diffraction measurement showed that the Lamellar d-spacing (d_1) of the out-of-plane PQCQT was 23.2 Å, and the π–π stacking distance (d_π) between the layers was 3.5 Å. A bulk-heterojunction type of polymer solar cell was produced with a structure of ITO/PEDOT:PSS/active-layer/PFN/Al. When the ratio of the PQCQT and $PC_{71}BM$ was 1:2, the device performed best with a power conversion efficiency (PCE) of 2.3%.

1. Introduction

In recent years, semiconducting polymers have been studied in a wide range of applications, such as organic light emitting diodes (OLEDs) [1–3], organic photovoltaic cells (OPVs) [4–10], and organic thin film transistors (OTFTs) [11–13]. Because OPVs have the possibility of economic validity and continuous development without environmental destruction in such applications, they are emerging into the spotlight as a global technology trend and taking center stage as an important research subject. Nevertheless, the low power conversion efficiency (PCE) has become the most significant obstacle in the field of OPVs [6].

To improve the PCE, the conjugated polymer requires the following ideal conditions: (1) low band gap with wide absorbance area, (2) crystalline structure for suitable charge transport properties, (3) low highest occupied molecular orbital (HOMO) energy level for the high open-circuit voltage (V_{oc}), and (4) appropriate lowest unoccupied molecular orbital (LUMO) energy level for the effective charge electron transfer to fullerene.

To ensure suitable charge transport properties among the polymers, the close packing between polymers should be increased through the reduction of the energetic disorder of polymers, which is caused by the increase in the coplanarity and π–π stacking of polymers. A PCE of 4.7% has been reported for the high hole mobility (0.04 $cm^2 V^{-1} S^{-1}$) in the copolymer of the terthiophene and diketopyrrolopyrrole derivatives; the Janssen Group showed the increase in planarity packing and high mobility property [14]. It has been reported that the copolymer, which introduces the indacenodithiophene (IDT) and phenanthrenequinoxaline units, had a hole mobility of 0.029 $cm^2 V^{-1} S^{-1}$ and a PCE of 6.2% in the Jen group [15]. In addition, the McCulloch group reported that the polymer introducing the benzo[1,2-b:3,4-b′:5,6-d′]trithiophene (BTT) derivatives with excellent intermolecular packing properties in its main chain had a hole mobility of 0.24 $cm^2 V^{-1} S^{-1}$ and a PCE of 2.2% [16,17].

Because quinacridone (QC) derivatives, commonly known as red–violet pigment, show high crystallizability and self-assembly properties, they are receiving attention as OTFTs with high mobility [18]. However, the results of such QC derivatives are for mainly small molecules and oligomers, and the polymer is extremely limited [19–21]. Recently, the Takimiya group reported the polymer containing quinacridone (QC) derivatives with a high hole mobility of 0.2 $cm^2 V^{-1} S^{-1}$ similar to that of OTFT materials [22]. Recently, we have synthesized PQCDTB, introducing the QC derivative as a donor and reporting its properties of self-organization [23].

In this study, we have synthesized a new poly[quinacridone–quaterthiophene] (PQCQT) containing the QC and quaterthiophene

* Corresponding author. Tel.: +82 2 450 3498; fax: +82 2 444 0765.
E-mail address: dkmoon@konkuk.ac.kr (D. K. Moon).

0927-0248/$ - see front matter © 2013 Elsevier B.V. All rights reserved.
http://dx.doi.org/10.1016/j.solmat.2013.05.057

(QT) derivatives. It is expected that this product will have effective self-organization and mobility properties due to its self-assembly and coplanarity.

2. Experimental section

2.1. Instruments and characterization

Unless otherwise specified, all reactions were conducted under a nitrogen atmosphere. The solvents were dried by standard procedures. All column chromatography was performed with the use of silica gel (230–400 mesh, Merck) as the stationary phase. ^{1}H-NMR spectra were obtained using a Bruker ARX 400 spectrometer using solutions in $CDCl_3$, and the chemical shifts were recorded in ppm units with TMS as the internal standard. The elemental analyses were measured with EA1112 using a CE Instrument. Electronic absorption spectra were measured in chloroform using an HP Agilent 8453 UV–vis spectrophotometer. The cyclic voltammetric waves were produced using a Zahner IM6eX electrochemical workstation at a constant scan rate of 50 mV/s with a 0.1 M acetonitrile (substituted with nitrogen for 20 min) solution containing tetrabutyl ammonium hexafluorophosphate (Bu_4NPF_6) as the electrolyte. The ITO, Pt wire, and silver/silver chloride [Ag in 0.1 M KCl] were used as the working electrode, counter electrode, and reference electrode, respectively. The electrochemical potential was calibrated against Fc/Fc^+. The HOMO levels of the polymers were determined using the oxidation onset value. Onset potentials are values obtained from the intersection of two tangents drawn at the rising current and baseline changing current of the CV curves. TGA measurements were performed on a NETZSCH TG 209 F3 thermogravimetric analyzer. All GPC analyses were made using THF as the eluent and a polystyrene standard as the reference. X-ray diffraction (XRD) patterns were obtained using SmartLab 3 kW (40 kV 30 mA, Cu target, wavelength: 1.541871 ang) in Rigaku, Japan. Topographic images of the active layers were obtained through atomic force microscopy (AFM) in tapping mode under ambient conditions using a XE-100 instrument. The theoretical study was performed by using the density functional theory (DFT), as approximated by the B3LYP functional and employing the 6-31G* basis set in Gaussian09.

2.2. Fabrication and characterization of polymer solar cells

All bulk-heterojunction PV cells were prepared using the following device fabrication procedure. The glass/indium tin oxide (ITO) substrates [Sanyo, Japan (10 Ω/γ)] were sequentially lithographically patterned, cleaned with detergent, and ultrasonicated in deionized water, acetone, and isopropyl alcohol. Then, the substrates were dried on a hotplate at 120 °C for 10 min and treated with oxygen plasma for 10 min to improve the contact angle before the film coating process. Poly(3,4-ethylene-dioxythiophene): poly(styrene-sulfonate) (PEDOT:PSS, Baytron P 4083 Bayer AG) was passed through a 0.45 μm filter before being deposited onto the ITO at a thickness of ca. 32 nm by spin-coating at 4000 rpm in air and drying at 120 °C for 20 min inside a glove box. Composite solutions with polymers and PCBM were prepared using 1,2-dichlorobenzene (DCB). The concentration was controlled adequately in the 0.5 wt% range, and the solutions were filtered through a 0.45 μm PTFE filter and spin-coated (500–2000 rpm, 30 s) on top of the PEDOT:PSS layer. The device fabrication was completed by depositing thin layers of BaF_2 (1 nm), Ba (2 nm), and Al (200 nm) at pressures of less than 10^{-6} Torr. The active area of the device was 4.0 mm^2. Finally, the cell was encapsulated using UV-curing glue (Nagase, Japan). In this study, all the devices were fabricated with the following structure: ITO glass/PEDOT:PSS/polymer:PCBM/BaF_2/Ba/Al/encapsulation glass.

The illumination intensity was calibrated using a standard Si photodiode detector equipped with a KG-5 filter. The output photocurrent was adjusted to match the photocurrent of the Si reference cell to obtain a power density of 100 mW/cm^2. After the encapsulation, all devices operated under an ambient atmosphere of 25 °C. The current–voltage (I–V) curves of the photovoltaic devices were measured using a computer-controlled Keithley 2400 source measurement unit (SMU) equipped with a Peccell solar simulator under an illumination of AM 1.5 G (100 mW/cm^2). The thicknesses of the thin films were measured using a KLA Tencor Alpha-step 500 surface profilometer with an accuracy of 1 nm.

The hole-only devices were fabricated with a diode configuration of ITO (170 nm)/PEDOT:PSS (40 nm)/PQCQT:PC_{71}BM (50 nm)/MoO_3 (30 nm)/Al (100 nm). The hole mobility of the active layers was calculated from the SCLC using the J–V curves of the hole-only devices in the dark as follows:

$$J = \frac{9}{8}\varepsilon_r\varepsilon_0\mu_{h(e)}\frac{V^2}{L^3}\exp\left(0.89\sqrt{\frac{V}{E_0L}}\right)$$

where ε_0 is the permittivity of free space (8.85×10^{-14} C/Vcm); ε_r is the dielectric constant (assumed to be 3, which is a typical value for conjugated polymers) of the polymer;$\mu_{h(e)}$ is the zero-field mobility of holes (electrons); L is the film thickness; and $V = V_{appl} - (V_r + V_{bi})$, where V_{appl} is the applied voltage to the device, V_r is the voltage drop due to series resistance across the electrodes, and V_{bi} is the built-in voltage.

2.3. Materials

All reagents were purchased from Aldrich, Acros or TCI companies. All chemicals were used without further purification. The following compounds were synthesized using modified literature procedures: 2,9-diboronic ester-N,N′-di(2-octyl-dodecyl)quinacridone (M1) [23] and 5,5′-bis(3-dodecylthiophen-2-yl)-2,2′-bithiophene (M2) [8].

2.3.1. Poly[quinacridone-alt-octyloxydithienylbenzothiadiazole] (PQCQT)

The 5,5′-bis(3-dodecylthiophen-2-yl)-2,2′-bithiophene (M2) (0.22 g, 0.27 mmol), 2,9-diboronic ester-N,N′-di(2-octyl-dodecyl) quinacridone (M1) (0.30 g, 0.27 mmol), $Pd(PPh_3)_4$(0) (0.009 g, 0.008 mmol) and aliquat336 compounds were placed in a Schlenk tube and purged with three nitrogen/vacuum cycles. Under nitrogen atmosphere, 2 M degassed aqueous K_2CO_3 (10 mL) and dry toluene (20 mL) were added. The mixture was heated to 90 °C and stirred in the dark for 24 h. After the polymerization was complete, the mixture was end-capped with bromothiophene. After reaction quenching, the entire mixture was poured into methanol. The precipitate was filtered off and purified via Soxhlet extraction in the following order: methanol, acetone and chloroform. The polymer was recovered from the chloroform fraction and precipitated into methanol. The final product was obtained after being dried in a vacuum. Dark black solid. (0.3 g, 71%) Anal. Calcd. for $C_{100}H_{148}N_2O_2S_4$: C, 78.07; H, 9.70; N, 1.82; S, 8.34; O, 2.08. Found: C, 79.35; H, 10.24; N, 1.90; S, 8.45; O, 3.42.

3. Results and discussion

3.1. Material synthesis

The chemical structure and synthetic process of monomers or polymers is shown in Scheme 1. The poly[quinacridone–quaterthiophene] (PQCQT) was synthesized by the Suzuki coupling

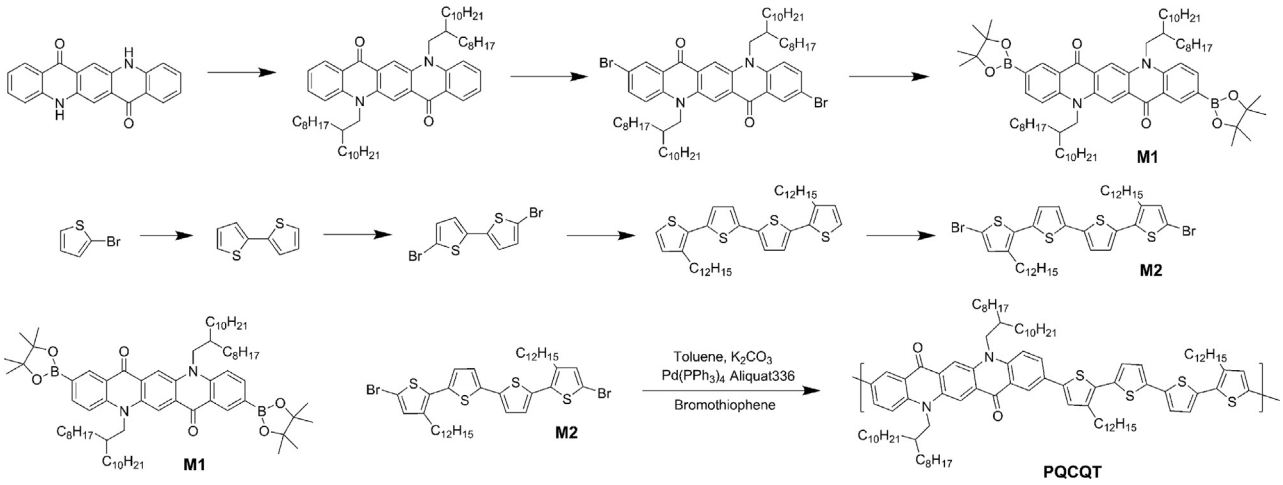

Scheme 1. Scheme of monomer synthesis and polymerization.

Table 1
Molecular weight and thermal properties of the polymers.

Polymer	M_n (kg/mol)	M_w (kg/mol)	PDI	T_d (°C)[a]
PQCQT	52.9	78.2	1.48	423

[a] Temperature resulting in 5% weight loss based on initial weight.

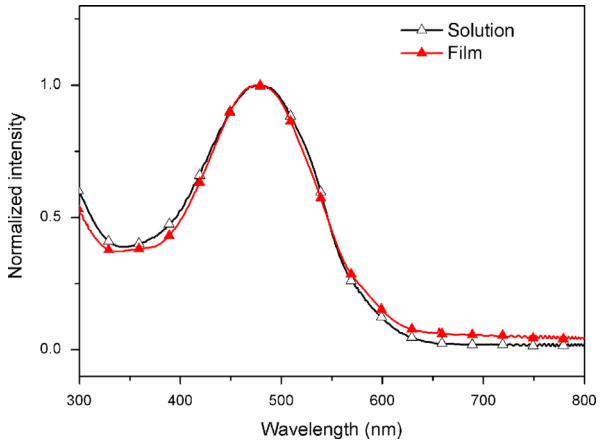

Fig. 1. Absorption spectra of PQCQT in solution (10^{-6} M) and film (50 nm).

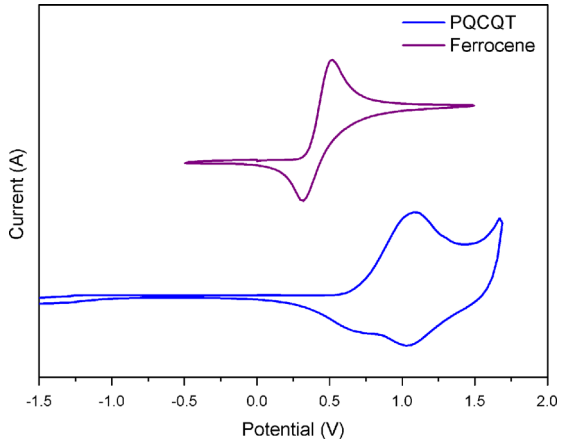

Fig. 2. Cyclic voltammogram of PQCQT.

reaction using M1 or M2, as shown in Scheme 1. The polymerization of palladium catalyst(0) and 2 M potassium carbonate solution was reacted at 90 °C for 24 h, using aliquot 336 as a surfactant and toluene as a solvent. After the synthesis was completed, the end-capping was performed by bromothiophene. The synthesized polymer was purified via Soxhlet extraction in the following order: methanol, acetone and chloroform. Then, the polymer was recovered from the chloroform fraction and precipitated into methanol, and the yield was 71%. The obtained polymer dissolved in the THF; however, the chloroform did not dissolve well in the chlorobenzene and o-dichlorobenzene. The uniform semitransparent red-colored film was formed via the spin-coating method.

The molecular weight and thermal properties of the PQCQT are shown in Table 1. As shown in this table, when the GPC was measured using polystyrene as the standard, the number-average molecular weight (M_n) of PQCQT was 52.9 kg/mol. In contrast, the polydispersity indices (PDI) showed a very narrow distribution of 1.48. The PQCQT was 2–3 times greater than the other OPV polymers because of the introduction of long, branched side chains of quinacridone and thiophene [6].

The results of the thermal analysis through TGA are shown in Table 1. The PQCQT had a high thermal stability because the 5 wt% loss point was approximately 423 °C, which was due to the rigid structure of the QC and QT, as shown in Table 1. This phenomenon has a potential application in OPVs, which require a high thermal stability of 300 °C or more, and the opto-electronic device field [21].

3.2. Optical and electrochemical properties

The UV–visible spectra of the PQCOT are presented in Fig. 1. The maximum absorption peak (λ_{max}) of the PQCQT appeared in the nearly overlapped form between 474 nm and 477 nm of the solution (10^{-6} M in $CHCl_3$) and film (50 nm thickness), as shown in Fig. 1. The planar quinacridone derivatives effectively reduce the steric hindrance; additionally, strong chain staking occurs due to the hydrogen bonding of the quinacridone [15]. The calculated optical band gap through the UV onset value of film was 2.12 eV, which is similar to that of the P3HT.

The cyclic voltammogram of the PQCQT measured from a 0.1 M tetrabutylammonium-hexafluoro-phosphate acetonitrile solution is shown in Fig. 2. The PQCQT showed an oxidation peak similar to that of PQA2T(poly quinacridone-bithiophene), as reported by Osaka, et al. [22]. This result occurs because the structure of the PQCQT is a typical p-type, similar to the PQA2T. The oxidation (E_{ox}^{onset}) onset potential of the PQCQT was +0.72 V. The optical and electrochemical properties of the polymers are summarized in

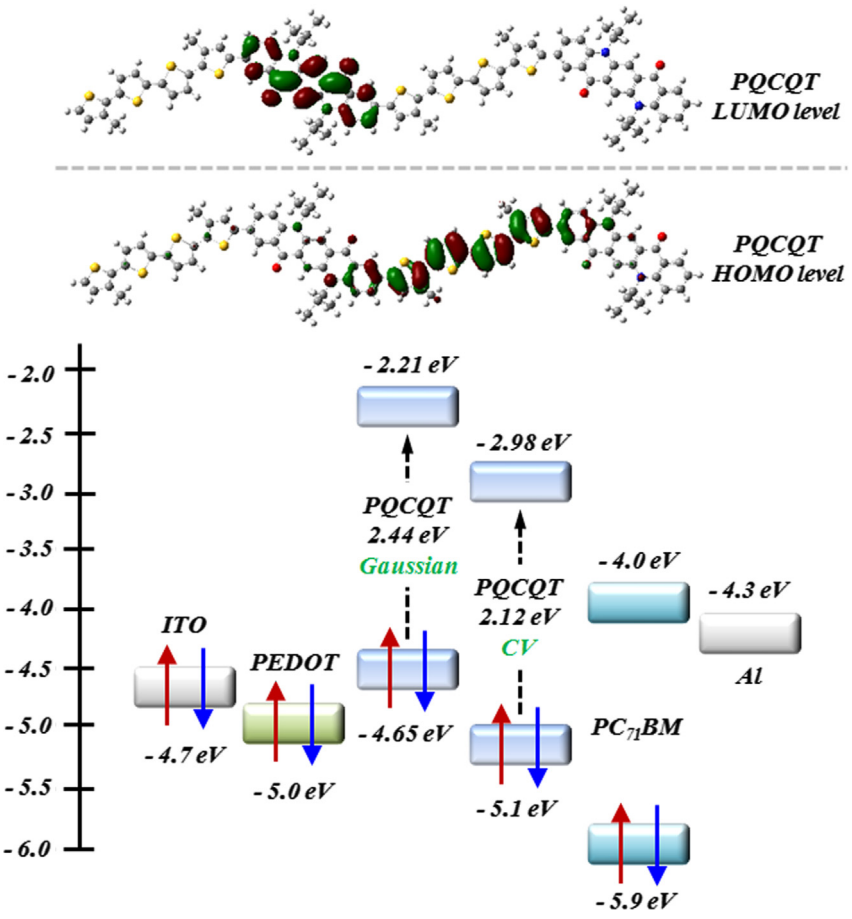

Fig. 3. DFT Gaussian simulation and band diagram of PQCQT (calculated and experiment level), ITO, $PC_{71}BM$, Al.

Table 2
Optical and electrochemical properties of the polymers.

Polymer	Absorption, λ_{max} (nm)		E_{ox}^{onset} (V)	E_{HOMO} (eV)[c]	E_{LUMO} (eV)[d]	E_{opt} (eV)[e]
	Solution[a]	Film[b]				
PQCQT	477	474	0.72	−5.10	−2.98	2.12

[a] Absorption spectrum in $CHCl_3$ solution (10^{-5} M).
[b] Spin-coated thin film (50 nm).
[c] Calculated from the oxidation onset potentials under the assumption that the absolute energy level of Fc/Fc^+ was −4.8 eV below a vacuum.
[d] HOMO–E_{opt}.
[e] Estimated from the onset of UV–vis absorption data of the thin film.

Table 2. The HOMO level of the PQCQT was −5.10 eV, which is similar to the PQA2T, as reported by Takimiya, et al. and shown in Table 2. The LUMO energy level was calculated from the difference between the HOMO energy level and the optical band gap energy. According to this calculation, the LUMO level of the PQCQT was −2.98 eV. The energy level of each material based on the results of the density functional theory (DFT) calculation and experimental results are shown as a band diagram in Fig. 3. According to the DFT calculation results, the energies of the HOMO and LUMO of the PQCQT were 4.65 eV and 2.21 eV, respectively. These results showed energies of 0.45 and 0.77 eV, which are higher than the results of the CV experiment but are similar to the trend described in other literature [24].

Because the HOMO energy of the PQCQT is lower than the P3HT HOMO energy (−4.9 eV), it explains the relatively high air stability [25]. In the case of the PQCQT, the LUMO level (−2.98 eV) was 0.68 eV higher than the $PC_{71}BM$ LUMO level (−4.0 eV). In addition, its value was −5.1 eV, which is 0.1 eV lower than the PEDOT:PSS HOMO level (−5.0 eV). Therefore, if the charge separation occurred by light harvest, the hole, rather than the electrons, would effectively show the charge transport [23,26].

3.3. Orientation analysis

Fig. 4 shows the results of the film X-ray diffraction measurement to analyze the ordering structure of the PQCQT. The samples for measurement were fabricated with a structure of the ITO glass/PEDOT:PSS/PQCQT layer, as shown in Fig. 4(b). The PQCQT layer was fabricated by drop casting with the PQCQT solution dissolved in the ODCB (10 mg/1 mL).

In the out-of-plane pattern, a sharp diffraction peak was observed at 3.8°, 7.7°, and 11.7°, which indicates the formation of ordered lamellar structure as the *a*-axis (h00) direction by the alkyl side chain of the quinacridone [22,23]. The lamellar d-spacing (d_1) was 23.2 Å ($\lambda = 2d\sin\theta$), which indicates that the PQCQT formed the conventional edge-on π stacking on the substrate and non-cubic structure, as shown in Fig. 4(b). Additionally, in the (010) in-plane pattern related to the π–π stacking, a broad diffraction peak was detected at approximately 24.5°. Using the same calculation, the π–π stacking distance (d_π) was 3.5 Å. The results are similar to the thiophene- and thiophene-fused aromatic system polymers that perform well as OPVs [22,27].

The tilt angle of the PQCQT was analyzed via the density functional theory (DFT) calculation. The tilt angles of the PQCQT were 22°, 18–21°, 0–1° and 18–21° among the linkage groups, as shown in Fig. 4(c). The tilt angle of the PQCQT was relatively low

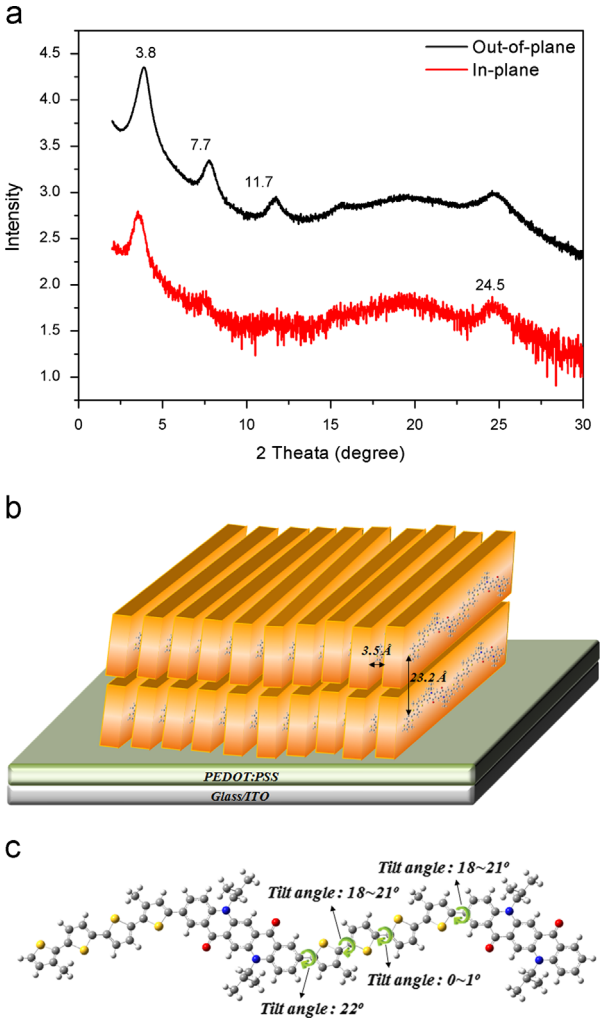

Fig. 4. (a) Out-of-plane and in-plane in X-ray diffraction pattern in thin films of thermal treatment (b) schematic representation of interdigitated packing structure and (c) tilt angles among each linkage group through DFT calculation.

compared to other benzene–thiophene linkages (27–28°). Thus, the π–π stacking of the PQCQT occurred effectively in comparison with other benzene–thiophene derivatives. This stacking was confirmed by XRD and is the result of the coplanar nature of the quinacridone unit introduced in the main chain of the PQCQT.

3.4. Photovoltaic characteristics

Fig. 5(a) and Table 3 show the results used to evaluate the manufacturing properties of the OPV device. The device structure was manufactured as ITO (170 nm)/PEDOT:PSS (40 nm)/active-layer (50 nm)/Al (100 nm). The active layer was dissolved in the polymer, and the PCBM was dissolved in the 0.5–1 wt% solution of o-dichlorobenzene (ODCB) and $CHCl_3$ (ODCB:$CHCl_3$ weight ratio=8:2) with 3% 1 8-diiodooctane (DIO) by volume. Then, the blending ratio was optimized. The photovoltaic performances of the fabricated OPVs were investigated under the illumination of AM 1.5G simulated solar light of 100 mW cm^{-2}. Because $PC_{71}BM$ absorbs many photons in the 400–500 nm wavelength range compared to $PC_{61}BM$, the PCE improved by increasing the J_{SC}; therefore, $PC_{71}BM$ was used as an acceptor [6].

As shown in Fig. 5(a) and Table 3, the V_{oc}, J_{sc}, FF and PCE values of the device blended in the 1:1 ratio of PQCQT to $PC_{71}BM$ were 0.59 V, 5.4 mA/cm^2, 34.5%, and 1.1%, respectively. Conversely, the V_{oc}, J_{sc}, FF and PCE values of the device blended in the 1:2 ratio of

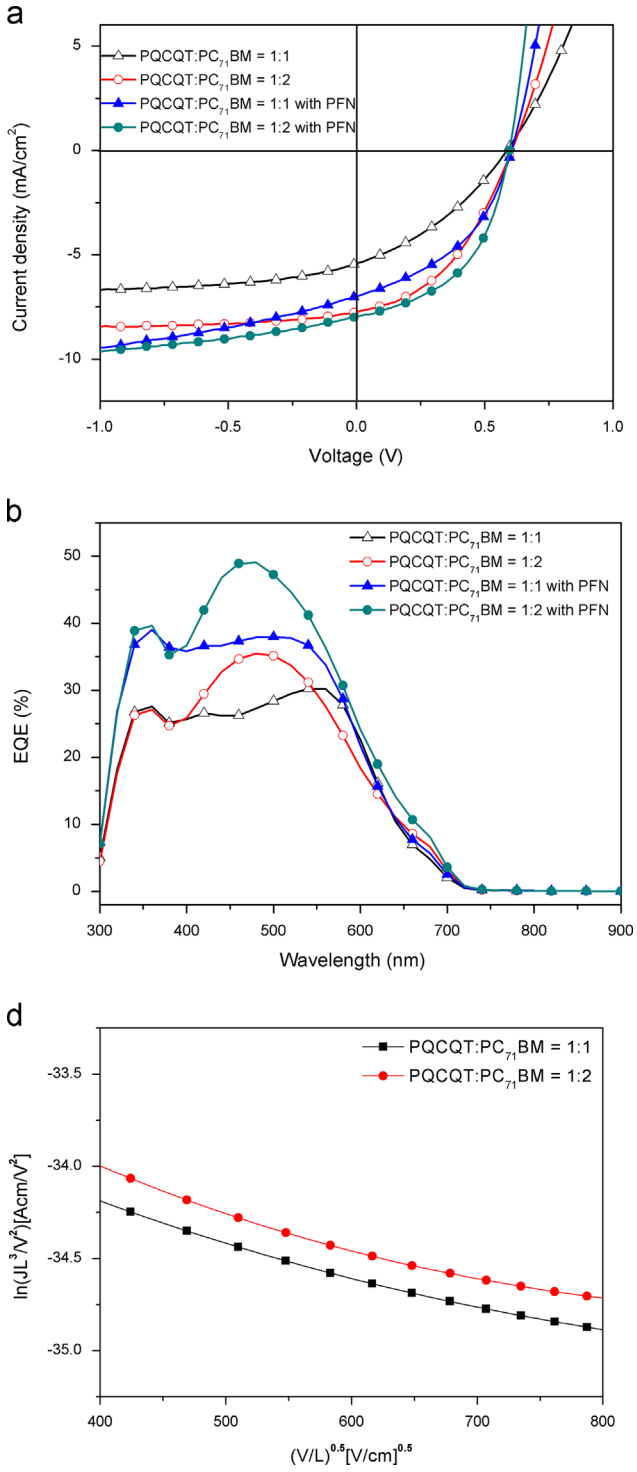

Fig. 5. (a) *J–V* characteristics, (b) EQE spectra of the BHJ solar cells with the device and (c) *J–V* characteristics of the hole-only devices (ITO (170 nm)/PEDOT:PSS (40 nm)/PQCQT:$PC_{71}BM$ (50 nm)/MoO_3 (30 nm)/Al (100 nm)).

PQCQT to $PC_{71}BM$ were 0.59 V, 7.7 mA/cm^2, 43.0%, and 2.0%, respectively. The V_{oc} of the PQCQT had a slightly higher value than the poly(3-hexylthiophene) (P3HT, V_{oc}=0.5–0.6 V), which is a commonly known donor material. This type of result was obtained because the HOMO level (−5.1 eV) of the PQCQT was lower than the HOMO level (−4.9 eV) of P3HT [25].

Recently, a number of studies were conducted to improve the performance of devices using poly[(9,9-bis(30-(N,N-dimethylamino)

Table 3
Photovoltaic performance of the BHJ solar cells with the device.

Active layer (w/w)		Weight ratio (P:A, w/w)	V_{OC} (V)	J_{SC} (mA/cm^2)	FF (%)	PCE (%)	R_s (Ω/cm^2)	R_{sh} (Ω/cm^2)
Polymer (P)	Acceptor (A)							
PQCQT	$PC_{71}BM$	1:1	0.59	5.4	34.5	1.1	33	201
		1:2	0.59	7.7	43.0	2.0	20	336
		1:1 with PFN	0.59	7.0	43.8	1.8	14	176
		1:2 with PFN	0.59	7.9	49.3	2.3	8	247

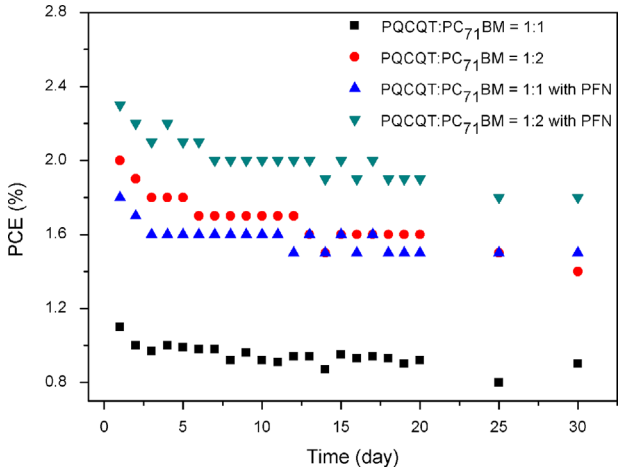

Fig. 6. Durability test data of photovoltaic devices based on ratio of PQCQT and $PC_{71}BM$.

propyl)-2,7-fluorene)-alt-2,7-(9,9-dioctylfluorene)] (PFN) because PFN improves the interfacial adhesion and electron transport between the active layers and cathodes [27]. Thus, we fabricated devices introducing PFN, and the results are summarized in Fig. 5(a) and Table 3. In the device structure, which consisted of ITO/PEDOT:PSS/active layer (PQCQT: $PC_{71}BM$=1:2)/PFN/Al, the values of V_{OC}, J_{SC}, FF, and PCE were 0.59 V, 7.9 mA/cm^2, 49.0%, and 2.3%, respectively. The device with PFN showed the best performance with improved J_{SC} and FF values compared with the device without PFN as the PFN interlayer improved the electron transport property between the active layers and Al.

To check the accuracy of the device measurements, the external quantum efficiency (EQE) of the device was measured; the EQE curve, including its ratio to $PC_{71}BM$, is shown in Fig. 5(b). The photons in the EQE curve occurred mostly in the polymer phase, which correlated with the absorption spectra of the polymers. The EQE curve was similar to the UV–vis spectrum shown in Fig. 1. The short-circuit current density for the PQCQT, which was determined from the EQE, compared with that of $PC_{71}BM$ (1:1 ratio with PFN) was 5.4 mA/cm^2. The theoretical short-circuit current density for the PQCQT (1:2 ratio with PFN), which was determined from the EQE, was 6.4 mA/cm^2. The EQE of the PQCQT (1:2 ratio) led to a larger current density than that of the 1:1 ratio due to the charge balance. However, there is a slight difference; the J_{SC} value of the device and the J_{SC} value of the IPCE showed a similar trend.

In BHJ solar cells, the hole mobility in the polymer is extremely important to their photovoltaic performance. We used a space charge limited current (SCLC) model to determine the hole mobility in blends with $PC_{71}BM$ [28]. The hole-only devices were fabricated with a diode configuration of ITO (170 nm)/PEDOT:PSS (40 nm)/ PQCQT:$PC_{71}BM$ (50 nm)/MoO_3 (30 nm)/Al (100 nm). Fig. 5(c) shows the *J–V* characteristics of the hole-only devices

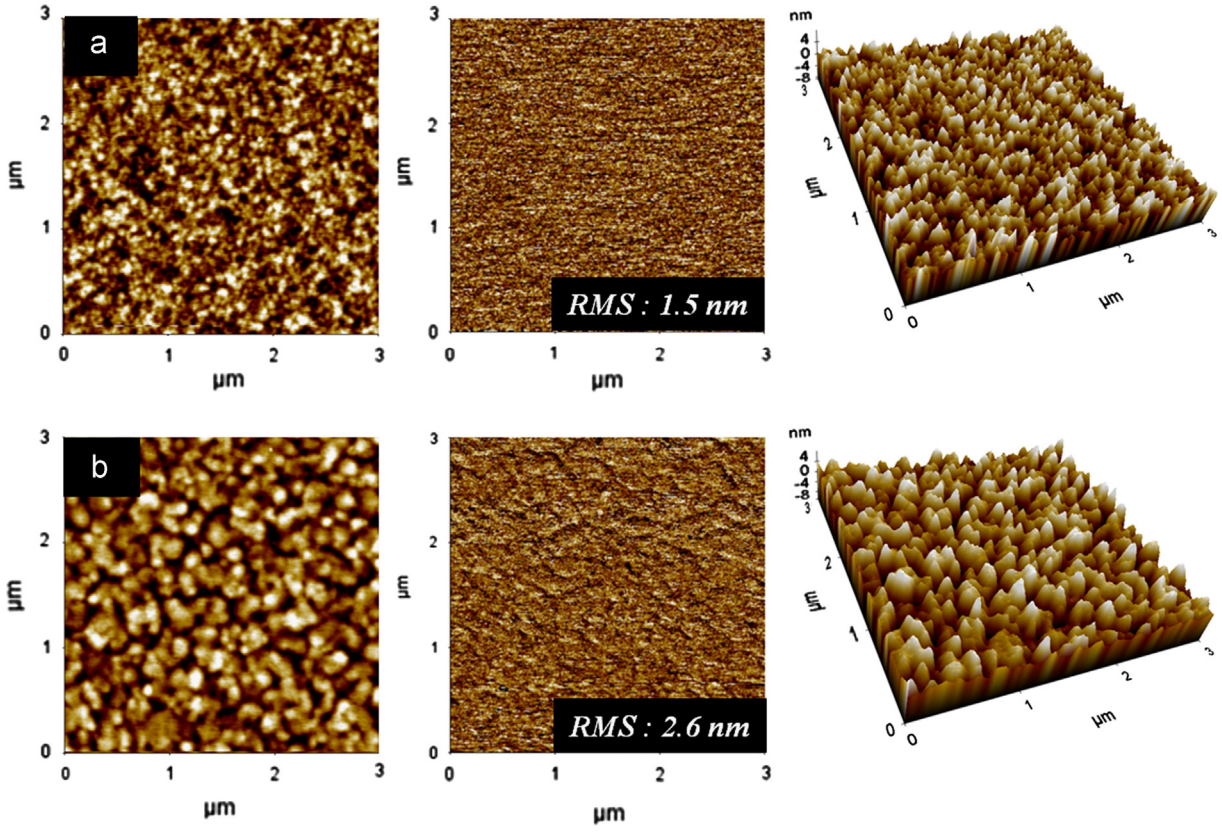

Fig. 7. Topographic AFM images of (a) PQCQT: $PC_{71}BM$ 1: 1 (3 × 3 μm^2) and (b) PQCQT: $PC_{71}BM$ 1: 2 (3 × 3 μm^2).

based on the PQCQT:$PC_{71}BM$ blends. The hole mobility of the PQCQT: $PC_{71}BM$ (1:1 ratio) was estimated to be approximately 4.70×10^{-3} cm^2 V^{-1} s^{-1}, while that of the PQCQT: $PC_{71}BM$ (1:2 ratio) was estimated to be approximately 3.85×10^{-3} cm^2 V^{-1} s^{-1}. The electron mobility (2×10^{-3} cm^2 V^{-1} s^{-1}) of the $PC_{71}BM$ was more similar to the hole mobility of the 1:2 ratio blend than that of the 1:1 ratio blend, resulting in a balance in the hole and electron transport in the 1:2 blended film ratio [28].

To investigate the oxidative stability of photovoltaic devices based on PQCQT, the current density–voltage (*J–V*) curves of the devices were measured under ambient conditions for one month [29]. All of the devices were encapsulated to prevent oxidation of the metal electrode and maintained under ambient conditions. As shown in Fig. 6, the PCE values of the devices based on the PQCQT as a donor material had changed slightly after one day. Moreover, the PCE values of these devices decreased by only approximately 20% after one month, which is likely due to the electrochemical stability of donor polymers, as mentioned above.

3.5. Morphology analysis

To investigate the morphology of the PQCQT/$PC_{71}BM$ blend film, atomic force microscopy (AFM) was conducted, and the result is represented in Fig. 7. In Fig. 7(a), because the ratio of PQCQT/$PC_{71}BM$ is 1:1, the polymer consists of a small domain and a fibril form, and the micro-phase separation between the polymer and $PC_{71}BM$ is shown simultaneously. The fibril domain, or micro-phase separation, was more evident when measured at a 1×1 μm^2 size (see Supplementary information). It is assumed that these fibril domains appeared as a result of the self-organization characterization of the PQCQT [30]. Conversely, as shown in Fig. 7(b), when the PQCDTB/$PC_{71}BM$ ratio was 1:2, the polymers were self-assembled, and a large domain was formed. As a result, a relatively large-size phase separation occurred. The large domain or the large-size phase separation was more evident when measured at a 1×1 μm^2 size (see Supplementary information).

4. Conclusions

We successfully synthesized the PQCQT through a Suzuki coupling reaction involving quinacridone and quaterthiophene units. The PQCQT polymer showed a high molecular weight and thermal stability; the air stability and band gap of 2.12 eV were attributed to the low HOMO energy level. As a result of the X-ray diffraction measurement, the Lamellar d-spacing (d_1) of the out-of-plane PQCQT was 23.2 Å, and the π–π stacking distance (d_π) between layers was 3.5 Å. In the device structure of ITO/PEDOT:PSS/active layer (PQCQT: $PC_{71}BM$ = 1:2)/PFN/Al, the values of V_{OC}, J_{SC}, FF, and PCE were 0.59 V, 7.9 mA/cm^2, 49.0%, and 2.3%, respectively. It is possible that more effective performance levels could be obtained if the chemical and device structures of the polymer were optimized.

Acknowledgments

This research was supported by a Grant from Fundamental R&D Program for Core Technology of Materials funded by Ministry of Knowledge Economy, Republic of Korea. This work was supported by the National Research Foundation of Korea Grant funded by the Korean Government (MEST) (NRF-2009-C1AAA001-2009-0093526).

Appendix A. Supporting information

Supplementary information associated with this article can be found in the online version at http://dx.doi.org/10.1016/j.solmat.2013.05.057.

References

[1] R.H. Friend, R.W. Gymer, A.B. Holmes, J.H. Burroughes, R.N. Marks, C. Taliani, D.D.C. Bradley, D.A.D. Santos, J.L. Bredas, M. Logdlund, W.R. Salaneck, Electroluminescence in conjugated polymers, Nature 397 (1999) 121–128.
[2] C.A. Breen, J.R. Tischler, V. Bulović, T.M. Swager, Highly efficient blue electroluminescence from poly(phenylene ethynylene) via energy transfer from a hole-transport matrix, Advanced Materials 17 (2005) 1981–1985.
[3] H.J. Song, J.Y. Lee, I.S. Song, D.K. Moon, J.R. Haw, Synthesis and electroluminescence properties of fluorene–anthracene based copolymers for blue and white emitting diodes, Journal of Industrial and Engineering Chemistry 17 (2011) 352–357.
[4] F.C. Krebs, Polymer solar cell modules prepared using roll-to-roll methods: knife-over-edge coating, slot-die coating and screen printing, Solar Energy Materials and Solar Cells 93 (2009) 465–475.
[5] E. Bundgaard, O. Hagemann, M. Manceau, M. Jørgensen, F.C. Krebs, Low band gap polymers for roll-to-roll coated polymer solar cells, Macromolecules 43 (2010) 8115–8120.
[6] J.-Y. Lee, S.-H. Kim, I.-S. Song, D.-K. Moon, Efficient donor-acceptor type polymer semiconductors with well-balanced energy levels and enhanced open circuit voltage properties for use in organic photovoltaics, Journal of Materials Chemistry 21 (2011) 16480–16487.
[7] M. Manceau, D. Angmo, M. Jørgensen, F.C. Krebs, ITO-free flexible polymer solar cells: from small model devices to roll-to-roll processed large modules, Organic Electronics 12 (2011) 566–574.
[8] H. Kong, S. Cho, D.H. Lee, N.S. Cho, M.-J. Park, I.H. Jung, J.-H. Park, C.E. Park, H.-K. Shim, The influence of electron deficient unit and interdigitated packing shape of new polythiophene derivatives on organic thin-film transistors and photovoltaic cells, Journal of Polymer Science Part A: Polymer Chemistry 49 (2011) 2886–2898.
[9] G. Li, V. Shrotriya, J. Huang, Y. Yao, T. Moriarty, K. Emery, Y. Yang, High-efficiency solution processable polymer photovoltaic cells by self-organization of polymer blends, Nature Materials 4 (2005) 864–868.
[10] F.C. Krebs, J. Fyenbo, M. Jorgensen, Product integration of compact roll-to-roll processed polymer solar cell modules: methods and manufacture using flexographic printing, slot-die coating and rotary screen printing, Journal of Materials Chemistry 20 (2010) 8994–9001.
[11] I. McCulloch, M. Heeney, C. Bailey, K. Genevicius, I. MacDonald, M. Shkunov, D. Sparrowe, S. Tierney, R. Wagner, W. Zhang, M.L. Chabinyc, R.J. Kline, M. D. McGehee, M.F. Toney, Liquid-crystalline semiconducting polymers with high charge-carrier mobility, Nature Materials 5 (2006) 328–333.
[12] T. Yamamoto, H. Kokubo, M. Kobashi, Y. Sakai, Alignment and field-effect transistor behavior of an alternative π-conjugated copolymer of thiophene and 4-alkylthiazole, Chemistry of Materials 16 (2004) 4616–4618.
[13] T. Yasuda, Y. Sakai, S. Aramaki, T. Yamamoto, New coplanar (ABA)n-type donor −acceptor π-conjugated copolymers constituted of alkylthiophene (unit A) and pyridazine (unit B): synthesis using hexamethylditin, self-organized solid structure, and optical and electrochemical properties of the copolymers, Chemistry of Materials 17 (2005) 6060–6068.
[14] J.C. Bijleveld, A.P. Zoombelt, S.G.J. Mathijssen, M.M. Wienk, M. Turbiez, D.M. de Leeuw, R.A.J. Janssen, Poly(diketopyrrolopyrrole−terthiophene) for ambipolar logic and photovoltaics, Journal of the American Chemical Society 131 (2009) 16616–16617.
[15] Y. Zhang, J. Zou, H.-L. Yip, K.-S. Chen, D.F. Zeigler, Y. Sun, A.K.Y. Jen, Indacenodithiophene and quinoxaline-based conjugated polymers for highly efficient polymer solar cells, Chemistry of Materials 23 (2011) 2289–2291.
[16] B.C. Schroeder, C.B. Nielsen, Y.J. Kim, J. Smith, Z. Huang, J. Durrant, S.E. Watkins, K. Song, T.D. Anthopoulos, I. McCulloch, Benzotrithiophene copolymers with high charge carrier mobilities in field-effect transistors, Chemistry of Materials 23 (2011) 4025–4031.
[17] C.B. Nielsen, B.C. Schroeder, A. Hadipour, B.P. Rand, S.E. Watkins, I. McCulloch, A benzotrithiophene-based low band gap polymer for polymer solar cells with high open-circuit voltage, Journal of Materials Chemistry 21 (2011) 17642–17645.
[18] X. Yang, J. Wang, X. Zhang, Z. Wang, Y. Wang, STM study on 2D molecular assemblies of luminescent quinacridone derivatives: structure fine-tuned by introducing bulky substitutes and co-adsorption with monofunctional/bifunctional acid, Langmuir 23 (2006) 1287–1291.
[19] J. Liu, B. Gao, Y. Cheng, Z. Xie, Y. Geng, L. Wang, X. Jing, F. Wang, Novel white electroluminescent single polymer derived from fluorene and quinacridone, Macromolecules 41 (2008) 1162–1167.
[20] J.J.-A. Chen, T.L. Chen, B. Kim, D.A. Poulsen, J.L. Mynar, J.M.J. Fréchet, B. Ma, Quinacridone-based molecular donors for solution processed bulk-heterojunction organic solar cells, ACS Applied Materials and Interfaces 2 (2010) 2679–2686.

[21] H.J. Song, S.M. Lee, J.Y. Lee, B.H. Choi, D.K. Moon, The synthesis and electroluminescent properties of dithienylquinacridone-based copolymers for white light-emitting diodes, Synthetic Metals 161 (2011) 2451–2459.
[22] I. Osaka, M. Akita, T. Koganezawa, K. Takimiya, Quinacridone-based semiconducting polymers: implication of electronic structure and orientational order for charge transport property, Chemistry of Materials 24 (2012) 1235–1243.
[23] H.-J. Song, D.-H. Kim, E.-J. Lee, S.-W. Heo, J.-Y. Lee, D.-K. Moon, Conjugated polymer consisting of quinacridone and benzothiadiazole as donor materials for organic photovoltaics: coplanar property of polymer backbone, Macromolecules 45 (2012) 7815–7822.
[24] N. Blouin, A. Michaud, D. Gendron, S. Wakim, E. Blair, R. Neagu-Plesu, M. Belletête, G. Durocher, Y. Tao, M. Leclerc, Toward a rational design of poly(2,7-carbazole) derivatives for solar cells, Journal of the American Chemical Society 130 (2007) 732–742.
[25] J. Hou, T.L. Chen, S. Zhang, L. Huo, S. Sista, Y. Yang, An easy and effective method to modulate molecular energy level of poly(3-alkylthiophene) for high-V_{oc} polymer solar cells, Macromolecules 42 (2009) 9217–9219.
[26] J.-M. Jiang, P.-A. Yang, T.-H. Hsieh, K.-H. Wei, Crystalline low-band gap polymers comprising thiophene and 2,1,3-benzooxadiazole units for bulk heterojunction solar cells, Macromolecules 44 (2011) 9155–9163.
[27] I. Osaka, T. Abe, S. Shinamura, E. Miyazaki, K. Takimiya, High-mobility semiconducting naphthodithiophene copolymers, Journal of the American Chemical Society 132 (2010) 5000–5001.
[28] S. Wen, J. Pei, P. Li, Y. Zhou, W. Cheng, Q. Dong, Z. Li, W. Tian, Synthesis and photovoltaic properties of low-bandgap 4,7-dithien-2-yl-2,1,3-benzothiadiazole-based poly(heteroarylenevinylene)s, Journal of Polymer Science Part A: Polymer Chemistry 49 (2011) 2715–2724.
[29] M.O. Reese, S.A. Gevorgyan, M. Jørgensen, E. Bundgaard, S.R. Kurtz, D.S. Ginley, D.C. Olson, M.T. Lloyd, P. Morvillo, E.A. Katz, A. Elschner, O. Haillant, T.R. Currier, V. Shrotriya, M. Hermenau, M. Riede, K.R. Kirov, G. Trimmel, T. Rath, O. Inganäs, F. Zhang, M. Andersson, K. Tvingstedt, M. Lira-Cantu, D. Laird, C. McGuiness, S. Gowrisanker, M. Pannone, M. Xiao, J. Hauch, R. Steim, D.M. DeLongchamp, R. Rösch, H. Hoppe, N. Espinosa, A. Urbina, G. Yaman-Uzunoglu, J.-B. Bonekamp, A.J.J.M. van Breemen, C. Girotto, E. Voroshazi, F.C. Krebs, Consensus stability testing protocols for organic photovoltaic materials and devices, Solar Energy Materials and Solar Cells 95 (2011) 1253–1267.
[30] B.-G. Kim, M.-S. Kim, J. Kim, Ultrasonic-assisted nanodimensional self-assembly of poly-3-hexylthiophene for organic photovoltaic cells, ACS Nano 4 (2010) 2160–2166.